HHS Public Access

Author manuscript

J Immunol. Author manuscript; available in PMC 2018 April 01.

Published in final edited form as:

J Immunol. 2017 April 01; 198(7): 2854–2864. doi:10.4049/jimmunol.1602006.

Reactive oxygen species-producing myeloid cells act as a bone marrow niche for sterile inflammation-induced reactive granulopoiesis

Haiyan Zhu[1,#], **Hyun-Jeong Kwak**[2,#], **Peng Liu**[1], **Besnik Bajrami**[2], **Yuanfu Xu**[1], **Shin-Young Park**[2], **Cesar Nombela-Arrieta**[2], **Subhanjan Mondal**[2], **Hiroto Kambara**[2], **Hongbo Yu**[4], **Li Chai**[3], **Leslie E. Silberstein**[2], **Tao Cheng**[1], and **Hongbo R. Luo**[2,*]

[1]The State Key Laboratory of Experimental Hematology, Institute of Hematology and Blood Diseases Hospital, Chinese Academy of Medical Sciences and Peking Union Medical College, 288 Nanjing Road, Tianjin, 300020, China

[2]Department of Pathology, Harvard Medical School; Department of Lab Medicine, Children's Hospital, Boston; Dana-Farber/Harvard Cancer Center, Boston MA 02115 USA

[3]Department of Pathology, Joint Program in Transfusion Medicine, Brigham and Women's Hospital, Harvard Medical School, Boston MA 02115 USA

[4]VA Boston Healthcare System, Department of Hematopathology, 1400 VFW Parkway, West Roxbury, MA 02132 USA

Summary

Both microbial infection and sterile inflammation augment bone marrow (BM) neutrophil production, but whether the induced accelerated granulopoiesis is mediated by a common pathway and the nature of such a pathway are poorly defined. We recently established that BM myeloid cell-derived reactive oxygen species (ROS) externally regulate myeloid progenitor proliferation and differentiation in bacteria-elicited emergency granulopoiesis. Here we show that BM ROS levels are also elevated during sterile inflammation. Similar to in microbial infection, ROS were mainly generated by the phagocytic NADPH oxidase in $Gr1^+$ myeloid cells. The myeloid cells and their ROS were uniformly distributed in the BM when visualized by multi-photon intravital microscopy, and ROS production was both required and sufficient for sterile inflammation-elicited reactive granulopoiesis. Elevated granulopoiesis was mediated by ROS-induced PTEN oxidation and deactivation leading to upregulated PtdIns(3,4,5)P3 signaling and increased progenitor cell proliferation. Collectively, these results demonstrate that although infection-induced emergency granulopoiesis and sterile inflammation-elicited reactive granulopoiesis are triggered by different

*To whom all correspondence should be addressed. Enders Research Building, Room 811, Boston, MA 02115, USA, Hongbo.Luo@childrens.harvard.edu, Phone: 617-919-2303, Fax: 617-730-0885.
#These authors contributed equally to this work.

Authorship Contributions

H. Kwak, P. Liu, B. Bajrami, and H. Zhu designed and carried out experiments, analyzed data and prepared manuscript. Y. Xu, C. Nombela-Arrieta, S. Park, H. Kambara, S. Mondal, L. Chai, L. Silberstein, and T. Cheng helped with designing experiments, analyzing data and evaluating manuscript. H. Luo designed experiments, analyzed data, and wrote paper.

Conflict of Interest Disclosures

The authors declare no competing financial interests.

stimuli and are mediated by distinct upstream signals, the pathways converge to NADPH oxidase-dependent ROS production by BM myeloid cells. Thus, BM $Gr1^+$ myeloid cells represent a key hematopoietic niche that supports accelerated granulopoiesis in both infective and sterile inflammation. This niche may be an excellent target in various immune-mediated pathologies or immune reconstitution after BM transplantation.

Introduction

Neutrophils are key players in innate immunity and host defense. During infection and inflammation, a large numbers of neutrophils are mobilized from the bone marrow (BM) to the circulation, and then recruited to affected tissues where they protect the host by recognizing, phagocytosing, and clearing invading pathogens. To compensate for their circulatory loss, BM granulopoiesis is enhanced during infection and inflammation.

Blood cells arise from self-renewing hematopoietic stem cells (HSCs) in the bone marrow (BM). Long-term HSCs (LT-HSCs) first differentiate to short-term HSCs (ST-HSCs). These ST-HSCs then give rise to more differentiated non-renewing multipotent progenitors (MPPs), common myeloid progenitors (CMPs), and common lymphoid progenitors (CLPs). CMPs gradually differentiate into megakaryocyte/erythroid progenitors (MEPs) and granulocyte/macrophage progenitors (GMPs). Although this classical hematopoietic hierarchy has long served as the conceptual framework for hematopoiesis research, recent studies using single-cell analyses indicate that progenitor populations including MPPs, CMPs, and MEPs are in fact heterogeneous and absent of mixed lineage progenitors (1, 2). It has also been reported that HSCs directly produce some self-renewing lineage-restricted progenitor cells (3).

Neutrophils are produced from GMPs through a series of developmental stages, including myeloblasts, promyelocytes, myelocytes, metamyelocytes, band neutrophils, and finally mature, segmented neutrophils (4). The process that maintain physiologic numbers of circulating neutrophils is known as “steady-state” granulopoiesis. The accelerated granulopoiesis that occurs during infection and inflammation is known as “emergency” granulopoiesis (5, 6). The two processes are regulated by distinct cellular mechanisms. For instance, the steady-state granulopoiesis is regulated by the C/EBP-alpha but not C/EBP-beta transcription factor (7, 8). In contrast, inflammation-induced accelerated granulopoiesis is largely controlled by C/EBP-beta but not C/EBP-alpha (8, 9).

Accelerated granulopoiesis is associated with both microbial infection-elicited emergency granulopoiesis and sterile inflammation-initiated reactive granulopoiesis (10). The two processes are triggered by different stimuli. Emergency granulopoiesis is dependent of the presence of a disseminated microbial pathogen. The pathogen-induced upregulation of myeloid differentiation pathways involves activation of toll-like receptor (TLR) signaling in the progenitors (11–13), although a recent report suggests that TLR-independent pathways can also mediate hematopoietic stem and progenitor cell expansion (14). In contrast, sterile inflammation associated reactive granulopoiesis is initiated by non-infectious stimuli such as chemical agents (e.g, acid, thioglycollate or alum), physical insults (e.g. trauma, surgery, burns or radiation) or autoimmune disorders (e.g. lupus or rheumatoid arthritis). Due to the

different upstream stimuli, there is also fundamental molecular differences between these two processes. For instance, the vaccine adjuvant alum induces reactive granulopoiesis in an IL-1 receptor 1 (IL-1R1) - dependent manner (9). Via activating IL-1RI mediated signaling, alum elicits a transient increase in G-CSF production which mobilizes neutrophils from the bone marrow. However, alum-induced accelerated granulopoiesis appears to be mediated by a density-dependent feedback that can sustain G-CSF level (15). Nevertheless, LPS-induced emergency granulopoiesis, which mimics microbial infection, is totally independent of IL-1R1 signaling (13).

Microbial infection and sterile inflammation can both accelerate granulopoiesis, suggesting that some molecular pathways might be shared between microbial infection-induced emergency and sterile inflammation-elicited reactive granulopoiesis. Extracellular granulopoietic factors such as interleukin-6 (IL-6), interleukin-6 (IL-3), granulocyte colony-stimulating factor (G-CSF), and granulocyte-macrophage colony-stimulating factor (GM-CSF), are implicated in both reactive and emergency granulopoiesis (8, 10, 16–21). However, infection-induced emergency granulopoiesis and sterile inflammation-elicited reactive granulopoiesis are triggered by different set of stimuli and are mediated by distinct upstream signals. Whether the induced accelerated granulopoiesis is mediated by a common intracellular pathway and the nature of such a pathway are poorly defined. We recently demonstrated that myeloid cell-derived ROS externally regulate the proliferation of myeloid progenitors in bacteria-elicited emergency granulopoiesis (22). Here we revealed that ROS also play a critical role in reactive granulopoiesis triggered by sterile inflammation. Although microbial infection-induced emergency granulopoiesis and sterile inflammation-elicited reactive granulopoiesis are triggered by different stimuli and mediated by distinct upstream signals, these pathways converge to a common point, namely NADPH oxidase-dependent ROS production by BM myeloid cells which accelerates granulopoiesis via upregulating PtdIns(3,4,5)P3 signaling. Collectively, we reveal a mechanism by which neutrophil homeostasis is rebalanced in response to acute sterile inflammation, and provide insights into a novel hematopoietic niche that might serve as a useful target in several pathologies such as chronic granulomatous disease or immune reconstitution after BM transplantation.

Methods

Mice

X-linked CGD mice (on C57BL/6 background) (29) that contain disrupted alleles of the gene encoding gp91phox were purchased from Jackson Laboratories. In this study, 8- to 12-week-old male mice were used. In all of the experiments performed with the CGD mice, we used C57BL/6 mice of the same age as WT controls. Every donor and recipient mouse used in the transplantation experiments was carefully genotyped for its CD45.1 and/or CD45.2 expression before the actual experiment. The numbers of mice analyzed per group for these transplant experiments are indicated in the figures; the data presented are a combination of three sets of separate experiments. Mice conditionally expressing EGFP (eGFP loxP/loxP) and the myeloid-specific Cre mice were purchased from Jackson Laboratories. Myeloid specific EGFP gene expression was achieved by breeding EGFP mice with myeloid specific

Cre mice (LyzM-EGFP mice). All animal manipulations were conducted in accordance with the Animal Welfare Guidelines of the Children's Hospital Boston. All procedures were approved and monitored by the Children's Hospital Animal Care and Use Committee.

Thioglycollate elicited peritoneal inflammation

CGD or wild-type mice were left uninjected or intraperitoneally injected with 1ml of 3% TG (Fluka) in distilled water. The differential peritoneal cell count was determined by microscopic analysis of Wright-Giemsa–stained cytospins (61). At various times after injection, the mice were sacrificed and inflammation induced granulopoiesis was analyzed using the BM cells.

Acid-induced acute lung injury

After anesthesia with ketamine hydrochloride (100 mg/kg intraperitoneally) and xylazine (10 mg/kg intraperitoneally), mouse trachea was surgically exposed, and a total volume of 50 μl of saline, or hydrochloric acid (0.1 N·HCl, pH 1.0; Sigma-Aldrich) was instilled intratracheally to the left bronchus. Colloidal carbon (1%) was included in the instillate to indicate deposition (62). At the end of the experiments, mice were euthanized by CO_2.

Hematologic analysis

Adult wild type and CGD mice were anesthetized and immediately bled retro-orbitally into an EDTA-coated tube. Complete blood counts were performed using an automated hematology analyzer (Hemavet 850; Drew Scientific, Oxford, CT). For BM cells, the total cell counts were determined using a hemacytometer, and the differential cell counts were conducted by microscopic analysis of Wright-Giemsa–stained cytospin or FACS analysis using CANTOII flow cytometer and FACSDiva software (BD Biosciences). The absolute number of neutrophils was then determined based on the cytospin or FACS analysis.

Flow cytometry and antibodies

Mice used for analysis were between 7 and 9 weeks old males. Single-cell suspensions of BM were obtained by crushing both tibias and femurs using a mortar and pestle and filtering through 40-μm cell strainers. Erythrocytes in the sample were lysed with an ACK lysis buffer (GibcoBRL). The cells were washed with a buffer containing 2% FCS in PBS. The antibodies used for flow cytometry included the following: APC-conjugated lineage markers specific for CD3e (145-2C110), CD4 (RM4–5), CD8a (53-6.7), CD11b(M1/70), B220 (RA3–6B2), GR-1 (RB6–8C5), and Ter119 (TER119) from eBioscience, Biolegend or BD pharmingen. Other antibodies included PC-Cy7- or FITC-conjugated Sca-1 (D7), APC-Cy7-conjugated c-kit (2B8), APC-conjugated CD45.2 (104), PE-Cy5-conjugated CD3e (145-2C11), PE-conjugated CD45.1 (A20), PE-conjugated CD36/32 (93), FITC-conjugated CD34 (RAM34). Unstained cells were used as negative control to establish the flow cytometer voltage setting, and single-color positive controls were used for adjustment of the compensation. The flow cytometric data were acquired using FACScalibar, and raw data were analyzed with Flowjo software (Treestar Inc). Hematopoietic stem cell population (HSC) was defined as $Lin^{-}IL\text{-}7R\alpha^{-}cKit^{+}Sca1^{+}$ (LSK) cells; hematopoietic progenitor cell (HPC) population was defined as $Lin^{-}IL\text{-}7R\alpha^{-}cKit^{+}Sca1^{-}$ (LK) cells; common lymphoid

progenitor (CLP) population was defined as Lin^- IL-7Rα^+c$Kit^{int}Sca1^{int}$ cells; common myeloid progenitor (CMP) population was defined as Lin^-IL-7Rα^- c-Kit^+Sca-1^-FcγII/III $R^{Int}CD34^+$ cells; granulocyte and monocyte progenitor (GMP) population was defined as Lin^-IL-7Rα^-c-Kit^+Sca-1^-FcγII/III R^+CD34^+ cells; and Megakaryocyte erythroid progenitor (MEP) was defined as FcγII/III $R^{low}CD34^{low}$c-Kit^+Sca-1^-IL-7Rα^- cells.

HSC and HPC sorting

Bone marrow cells were resuspended in 3 ml IMDM buffer and loaded on the top of Histopaque 1083 (Sigma-aldrich) to prepare low density bone marrow cells. Briefly, cells were centrifuged for 25 min at 1700 rpm with the brake off. The intermediate cell layer was removed and transferred to a 50 ml tube. Cell suspension was then centrifuged for 5 min at 1500 rpm and cell pellet was resuspended in 1 ml PBS with 2% PBS. For sorting, cells were stained with the APC-conjugated lineage-specific markers, PE-conjugated c-kit (2B8) and FITC-conjugated Sca-1 (D7). Cells were then sorted through a Lin-c-kit+Sca-1+ for LSK or Lin-c-kit+Sca-1- for LK cells, using FACS AriaII equipped with FACSDiva software (BD Bioscience).

Granulocyte/Monocyte Colony forming Unit (CFU-GM) assays

Bone marrow cells (2×10^4) from WT or CGD mice were seeded in semisolid Methocult GF M3534 medium containing rmSCF, rmIL-3 and rhIL-6 for detection of CFU-GM (Stem Cell Technologies). Number of colonies that contained more than 50 cells was counted on day 7. Colony numbers from 20,000 BMMCs are shown. The size of the colonies was also measured on day 7. Colony morphology was scored on the basis of Stemcell Technologies criteria. L-butionine-sulfoxamine (BSO, Sigma-Aldrich) was added to methylcellulose media at the indicated concentrations at the time of plating.

Detection of hydrogen peroxide using Amplex Red

ROS accumulation in the bone marrow during acute inflammation was measured in freshly isolated bone marrow using an Amplex red Hydrogen Peroxide assay Kit. Amplex Red (Invitrogen), a H_2O_2-sensitive fluorescent probe, was prepared according to the manufacturer's instructions. WT and CGD mice were intraperitoneally injected with 1 ml of 3% Thioglycollate in PBS. At the indicated times, mice were euthanized and BM were prepared by spinning femurs and tibias with 100 μl Krebs-Ringer phosphate buffer containing 5.5 mM glucose (pH 7.35). After further centrifugation (180*g* for 5 minutes) of the collected BM samples, the BM supernatant (extracellular ROS) was harvested and 50 μl was assayed (in duplicated) in 96-well fluorescent assay plates (Thermo Fisher Scientific) containing 50 μl/well Amplex Red solution with 0.2 U HRP. Fluorescence was recorded using a fluorometer (excitation, 540 nm; emission, 590 nm). The concentration of H_2O_2 was determined using a standard curve.

Analysis of *in vivo* cell proliferation by BrdU or EdU incorporation

Cell proliferation was determined using a BrdU labeling kit (BD bioscience) or a Click-iT™ Plus EdU Flow Cytometry Assay Kits (Invitrogen). Twenty four hours before sacrifice, BrdU was administrated by intraperitoneal injection (2 mg/mouse in 200 μl PBS) as a single

dose. At indicated time points, LSK, GMP, CMP, MEP cells were sorted from BM BMMC. Sorted cells were fixed in 70% ethanol overnight at –20°C, denatured in 2N HCl/0.5% Triton X-100 for 20 minutes at room temperature, neutralized with 0.1 M sodium borate for 5 minutes, and stained with anti-BrdU antibody (BD Biosciences, MD USA) for 30 minutes at room temperature in PBS/0.5% BSA/0.5% Tween 20. Cells were then resuspended in 500 μl PBS containing 10 μg RNase A and 5 μg Propidium Iodide (PI), incubated for 30 minutes, and immediately analyzed by flow cytometry. The mean frequencies of BrdU+ cells in the HSC and each progenitor populations were measured. For the EdU incorporation assay, EdU was administrated by intraperitoneal injection (0.5 mg/mouse in 200 μl PBS) as a single dose 24 hr before sacrificing the mice. The isolated cells were prepared and stained following a protocol provided by the manufacturer ((Invitrogen).

Neutrophil depletion with Gr-1 antibody

Neutrophil depletion was achieved by intraperitoneal injection of anti-Gr1 mAb RB6–8C5 (200 μg/kg). The antibody was administered i.p. to obtain a sustained depletion over the first 48 hours of the experiment. Differential white blood cell count using Wright-Giemsa staining was performed to confirm that the neutrophil depletion was successful.

G-CSF treatment and neutralization by anti-G-CSF antibody

Recombinant G-CSF (Amgen) was diluted in sterile PBS. G-CSF was administered by subcutaneous injection (250 μg/kg body weight). Bone marrow cells and peripheral blood were collected 24 hours following the G-CSF administration. Hydrogen peroxide production in the BM was measured as described above. To neutralize G-CSF *in vivo*, mice were injected subcutaneously with 100 μg anti-mouse G-CSF antibody (R & D system, clone67604). Hematopoietic cell lineage analysis and hydrogen peroxide measurement were conducted 24 hours following the antibody administration.

BM cell transplantation

Age-matching C57BL/6 and CD45.1 mice were purchased from Jackson Laboratories. Donor (CD45.1 mice) whole BM cells (WBM) were prepared by spinning femurs and tibias under sterile conditions, and red blood cells were lysed using ACK lysing buffer. LK progenitor cells were sorted using a FACS AriaII equipped with FACSDiva software (BD Bioscience) as previously described (63). The transplantation was conducted using non-irradiated WT (CD45.2) and CGD (CD45.2) recipient mice. The donor LK cells (CD45.1, 2×10^5) were transplanted into each non-irradiated WT (CD45.2) and CGD (CD45.2) recipient mouse via tail vein injection. To increase the efficiency of engraftment, LK cells were transplanted into recipient mice every 2 days for 1 wk. Hematopoietic chimerism was analyzed by FACS. In both WT and CGD recipient mice, donor CD45.1 LK cells successfully engrafted with stable chimerism of about 0.4% over 6 weeks. The acute peritonitis was induced using TG (3%) 6 weeks after the first BM transplantation. The emergency granulopoiesis elicited by inflammation was assessed 36 hr after the TG injection.

PTEN oxidation and Akt activation in the progenitor cells analyzed by western blotting

Wild-type and CGD mice were treated with 3% TG (PBS as control) or 1×10^6 *E.coli* (PBS as control) intraperitoneally for 24 hrs. LK cells were sorted using a FACS AriaII cell sorter. To obtain enough materials for western blotting, three mice were used for one data point in one single experiment. The sorted LK cells from each of the 3 mice were put together and half million LK cells were used for the assay. The cell pellets were lysed with 1x lysis buffer (30% 4x Invitrogen Nu-Page LDS buffer, 6% b-mercaptoethanol and 8% protease inhibitor cocktail in PBS, 95C). Cell extracts were resolved on Nu-Page 4–12% Bis-Tris gels, transferred onto PVDF membranes and then immunoblotted against S473P–Akt antibody (1:1000) or Akt antibody (1:5000). Densitometry of the blots was performed using the ImageJ software Gel Analyzer plugin. Phospho-Akt levels were then normalized based on total Akt levels (24). For PTEN oxidation analysis, the cell pellets were lysed with non-reducing LDS loading buffer. Cell extracts were then resolved on non-reducing SDS-PAGE. Both reduced and oxidized PTEN could be detected using a specific PTEN antibody(33).

Two-photon intravital microscopy

Mice were anesthetized with ketamine hydrochloride (100 mg/kg intraperitoneally) and xylazine (10 mg/kg intraperitoneally) and frontoparietal skull bone was exposed and prepared following previously established protocols (64). Two-photon microscopy on the calvarium bone marrow was performed using an Olympus BX50WI fluorescence microscope equipped with a 20×, 0.95 numerical aperture objective (Olympus) and a Bio-Rad Radiance 2000MP Multiphoton system, controlled by Lasersharp software (Bio-Rad). For two-photon excitation and second harmonic generation, a MAiTai Ti:sapphire laser was tuned to a range of wavelengths from 800 nm to 875 nm. The blood vesicles were labeled with Tetramethylrhodamine-dextran (Invitrogen, 2,000,000 MW). Myeloid cells in the mice expressing EGFP (LyzM-EGFP) were detected via eGFP-fluorescence and bone was visualized by its second harmonic generation signal. To detect H2O2 in the BM, PO1 (0.1mM in 100 μl PBS, a generous gift from Cris Chang, UC Berkley) was injected intravenously. Images were recorded every 30–40 sec for 10 minutes. The generated sequences of image stacks were transformed into volume-rendered four-dimensional movies using Volocity® (Perkin Elmer/Improvision) which was also used for tracking of cell motility in three dimensions.

Immunofluorescent staining and laser scanning cytometry of BM sections

Mice were perfused post-mortem with 10 ml paraformaldehyde-lysine-periodate (PLP) fixative through the vena cava to achieve rapid *in situ* fixation and optimal preservation of the bone marrow tissue. Femoral bones were isolated, fixed in PLP for 4–8 hours, rehydrated in 30% sucrose/PBS for 48 hours and snap frozen in OCT (TissueTek). Cryosections of non-decalcified whole longitudinal femoral bones were obtained using a Leica Cryostat and the Cryojane tape transfer system (Leica Microsystems). Bone marrow sections were stained with the indicated antibodies. DAPI (Invitrogen) staining was used for nuclear detection and sections were mounted with Vectashield mounting medium for immunofluoresence (Vector Labs). High resolution images of whole longitudinal immunostained femoral sections were obtained with a iCys Research Imaging Cytometer (Compucyte Corporation) equipped with

four laser lines (405, 488, 561 and 633 nm) and four PMT detectors with bandpass emission filters at 450/,40, 521/15, 575/50 and 650LP.

Neutrophil recruitment in the lungs

Wild-type and CGD mice were anesthetized and instilled with HCl as described above. After 24h mice were euthanized by CO_2. The chest cavity was opened, and a catheter was tied to the trachea. Bronchoalveolar lavage (BAL) was performed (1 mL of PBS/15mM EDTA ×10) in each group. The BAL fluid (BALF) was centrifuged at 450 *g* for 10 min, and the total and differential cell counts were determined from the pelleted cell fraction (62). The number of neutrophils in BALF was quantified by morphometric analyses of the Wright-Giemsa stained BALF cells. For morphometric examinations, investigators were blinded to the identities or the treatment of the mice.

Statistical analysis

Results are presented as means with error bars indicating the standard deviation (SD). Differences between groups were tested with the Student's t-test unless noted otherwise. P-values <0.05 were considered statistically significant. The normality of the data was confirmed by the Shapiro-Wilk normality test. All statistical tests and graphics were made using GraphPad Prism (GraphPad, San Diego, CA) or SPSS Statistics (IBM, Armonk, New York) software.

Results

Sterile inflammation augments granulopoiesis

To study reactive granulopoiesis during sterile inflammation, we used a mouse thioglycollate (TG) - elicited peritonitis model (23, 24). TG is a polysaccharide mixture. It is commonly used to induce acute mild peritonitis. As a result of TG-induced acute peritoneal inflammation, neutrophils were mobilized from the BM, resulting in an elevated peripheral blood neutrophil count and a decreased BM neutrophil count (Figure 1A and Figure S1A). After this initial instant reduction in BM neutrophils, the BM neutrophil count gradually increased, indicating inflammation-induced granulopoiesis (Figure 1A). To ensure that the TG-elicited effects were not due to endotoxin contamination, TG endotoxin levels were measured and were found to be much lower than those that would be expected to elicit a detectable response in mice (Figure S1B).

We next examined whether TG-induced sterile inflammation alters the number of hematopoietic progenitor cells using fluorescence-activated cell sorting (FACS) analysis. Similar to observations in bacteria-elicited emergency granulopoiesis (22), the percentage of GMPs ($Lin^{-}Sca\text{-}1^{low}c\text{-}Kit^{+}CD34^{+}Fc\gamma R^{high}$), but not CMPs ($Lin^{-}Sca\text{-}1^{low}c\text{-}Kit^{+}CD34^{+}Fc\gamma R^{low}$) or MEPs ($Lin^{-}Sca\text{-}1^{low}c\text{-}Kit^{+}CD34^{-}Fc\gamma R^{-}$), increased significantly after TG challenge (Figure 1B). Thus, TG-induced sterile inflammation specifically modulates myelopoiesis, and the GMP increase suggests that differentiation and proliferation of myeloid progenitor cells is specifically enhanced in TG-treated mice (Figure 1B). Interestingly, and similar to previously reported (25, 26), TG-elicited inflammation also led to a significant expansion of LSK ($Lin^{-}Sca\text{-}1^{+}c\text{-}Kit^{-}$ HSCs) cells (Figure S1C).

Consistent with specific GMP amplification, TG specifically augmented bromodeoxyuridine (BrdU) incorporation in GMPs, indicating elevated proliferation rate in this population (Figure 1C). Finally, BM from TG-treated mice contained more granulocyte–monocyte colony-forming units (CFU-G, CFU-M, and CFU-GMs) (>60/20000 BM cells) than untreated controls (about 40/20000 BM cells). Colonies originating from TG-treated animals (>250 μm in diameter) were also significantly larger than control colonies (about 150 μm in diameter) (Figure 1D). Collectively, all these results indicate that TG-induced sterile inflammation can elevate granulopoiesis.

ROS levels are elevated in the BM during TG-induced sterile inflammation

ROS are key mediators of bacteria-elicited emergency granulopoiesis (22). To explore whether ROS also play a role in TG-induced reactive granulopoiesis, we first measured ROS levels in the BM using Amplex® Red. During TG-induced acute sterile inflammation, BM extracellular space H_2O_2 levels increased gradually, peaking by 48 h (Figure 2A and Figure S1D). The results were similar when H_2O_2 was measured using another H_2O_2-specific probe, Peroxy Orange 1 (PO1), by multi-photon intravital microscopy (MP-IVM) of the BM microenvironment in live animals (Figure 2B). The BM cavity in the frontoparietal skull was imaged and analyzed using MP-IVM five minutes after intravenous PO1 injection, and mice challenged with TG for 24 h had significantly greater PO1 staining. Noticeably, in mice treated with 5FU, the neutrophil count was reduced. However, the bone marrow ROS level was not increased during the neutrophil recovery phase (Figure S1E). Similarly, depletion of neutrophils with anti-Gr1 Ab failed to augment the BM ROS level (Figure S1F). These results suggest that the induction of marrow ROS during inflammation is likely mediated by inflammatory factors, but not simply due to rapid granulopoiesis caused by stress of neutropenia.

Phagocytic NADPH oxidase is responsible for TG-elicited ROS production in the BM

Myeloid cells produce large amounts of ROS during acute infection and inflammation. These ROS are mainly generated by phagocytic NADPH oxidase (NOX2), and their classical function is to facilitate phagocytic killing of pathogens during infection (27, 28). To explore whether phagocytic NADPH oxidase is critical for TG-elicited ROS production, ROS levels were measured in TG-challenged chronic granulomatous disease (CGD) mice, in which the NADPH oxidase holoenzyme gp91 subunit is disrupted (29, 30). NOX2 deficiency significantly reduced BM ROS level in TG challenged mice (Figure 2C–D). TG-induced ROS production was likely to be mediated by $Gr1^+$ myeloid cell, since depletion of these cells with Gr1 antibodies abolished TG-elicited ROS production (Figure S1D). Indeed, over half of the cells in the BM were myeloid, with acute inflammation-elicited H_2O_2 production adjacent to these myeloid cells (Figure 2E). We previously showed that every BM c-Kit+ progenitor cells are adjacent to at least one Gr1+ myeloid cell (22), thus these progenitors are all surrounded by ROS in the BM.

ROS are required for TG-induced reactive granulopoiesis

NADPH oxidase-mediated ROS appeared to be essential for TG-induced reactive granulopoiesis. TG-elicited GMP (Figure 3A–B) and LSK cell (Figure S2A) expansion was completely abolished in CGD mice. In addition, disruption of NADPH oxidase inhibited

TG-induced increase of cell proliferation rate in the GMP population (Figure 3C). Consistently, CFU-GM assay show that inhibition of NOX2-dependent ROS production significantly decreased the number of BM myeloid progenitor cells (Figure 3D). Homeostatic signals have been proposed to promote progenitor proliferation in response to the loss of bone marrow neutrophils (15). We examined neutrophil count in the peripheral blood (Figure S2B) and neutrophil recruitment to the inflamed peritoneal cavity (Figure S2C) shortly after the TG injection, and did not detect any difference between the WT and CGD mice. This suggests that NOX2-mediated ROS production was not required for neutrophil mobilization from the BM. Thus the impaired TG-induced reactive granulopoiesis observed in the CGD mice was not due to alteration of neutrophil mobilization and the subsequent homeostatic signals. Previous study shows that reducing ROS level with ROS scavenger N-acetyl-cysteine (NAC) in myeloid progenitor cells suppresses the colony forming capability of the progenitors *in vitro* (22). We next used NAC to examine the involvement of ROS in reactive granulopoiesis. NAC treatment effectively reduced ROS levels *in vivo* in TG-challenged mice (Figure S2D), and suppressed TG-elicited GMP (Figure 3E–F) and LSK cell (Figure S2E) expansion, confirming that ROS are required for TG-induced reactive granulopoiesis.

ROS accelerate proliferation of myeloid progenitor cells to levels comparable to TG-induced granulopoiesis

L-buthionine-S,R-sulfoximine (BSO), an inhibitor of GSH biosynthesis, has been used to augment intracellular ROS levels in cultured myeloid progenitors (22). Myeloid progenitor cell proliferation is clearly enhanced by high ROS concentrations. BSO also elevated ROS levels *in vivo*. BSO treatment increased BM ROS levels over three-fold in both WT and CGD mice (Figure 4A). Consequently, GMP (Figure 4B–C) and LSK (Figure 4D) populations in the BM were significantly expanded in both WT and CGD mice, suggesting that the effect of BSO is independent of NADPH oxidase. In addition, NAC treatment counteracted the effect of BSO, confirming that the of action of BSO was indeed mediated by ROS induction. Importantly, BSO-induced granulopoiesis was largely comparable to TG-elicited reactive granulopoiesis, suggesting that TG-induced proliferation of myeloid progenitor cells may be solely mediated by ROS. Noticeably, BSO treatment did not induce neutrophil mobilization. The peripheral blood neutrophil count remained unaltered in the first 4 hr after the BSO treatment. The BSO treatment indeed elevated neutrophil count at later time point (24 hr) as a result of proliferative response of progenitors (Figure 4E). Finally, BSO alone did not induce G-CSF production. Thus BSO-induced increase of ROS level *in vivo* appeared to be sufficient to elicit reactive granulopoiesis and neutrophilia independent of G-CSF (Figure 4F).

TG-induced reactive granulopoiesis is mediated by PTEN oxidation and the subsequent upregulation of PtdIns(3,4,5)P3 signaling

We next explored the mechanism by which ROS mediate reactive granulopoiesis. One target of ROS-elicited protein modification is phosphatase and tensin homolog (PTEN), a lipid phosphatase that negatively regulates PtdIns(3,4,5)P3 signaling. PTEN's role in hematopoiesis and bacteria-induced emergency granulopoiesis is well documented (22, 31, 32). In various cell types, ROS can oxidize and inhibit PTEN activity and consequently

upregulate PtdIns(3,4,5)P3 signal pathway. Consistently, PTEN oxidation in LSK cells was detected on a non-reducing SDS-PAGE gel based on oxidation-induced mobility shift (33). TG-treatment significantly increased the level of PTEN oxidation in LK cells (Figure 5A). Disruption of NADPH oxidase prevented PTEN oxidation *in vivo*, confirming that this PTEN posttranslational modification event in the LK cells was mainly mediated by NADPH oxidase in myeloid cells (Figure 5B). It has been reported that PTEN oxidation inhibits PTEN's lipid phosphatase activity and in doing so upregulates PtdIns(3,4,5)P3 signal pathway. To establish whether this occurs in LK progenitor cells, PtdIns(3,4,5)P3 signal was measured using Akt phosphorylation as a reporter (Figure 5C). PtdIns(3,4,5)P3-dependent Akt phosphorylation in sorted WT LK progenitor cells was elevated over four-fold (30 h) in TG-induced sterile inflammation. This elevation was abolished in progenitor cells isolated from CGD mice (Figure 5C). NAC inhibited TG-elicited upregulation of Akt phosphorylation, while BSO augmented Akt phosphorylation even in the absence of TG challenge, indicating that ROS production was both required and sufficient for upregulation of PtdIns(3,4,5)P3 signal pathway (Figure 5D). Finally, treatment with a pan-PI3K inhibitor LY294002 and a specific PI3Kδ inhibitor IC87114 both reduced TG-induced GMP expansion (Figure 5E) and LSK (Figure S2F) cells. This suggests that upregulation of PtdIns(3,4,5)P3 signaling was essential for reactive granulopoiesis. It is noteworthy that PI3Kγ inhibitor AS605240 did not affect reactive granulopoiesis (Figure 5E), confirming that PtdIns(3,4,5)P3 signaling in the progenitors was mainly maintained by PI3Kδ which is downstream of receptor tyrosine kinases (34). Taken together, our results demonstrate that PTEN and PtdIns(3,4,5)P3/Akt signal pathways are a major players in TG-induced and ROS-mediated reactive granulopoiesis.

Myeloid-derived ROS externally regulate reactive granulopoiesis via a paracrine mechanism

ROS elevation during TG-induced sterile inflammation is predominately mediated by phagocytic NADPH oxidase which is mainly expressed in the BM myeloid cells. NADPH oxidase is gradually expressed during myelopoiesis. We have previously shown that $Gr1^+$ cells are uniformly localized in the BM, and Kit^+ stem and progenitor cells are all close to evenly distributed $Gr1^+$ cells (<50μm) (22). Thus, the sterile inflammation-induced expansion and differentiation of the myeloid progenitors can be regulated by ROS generated in the progenitor cells in an autonomous manner, or by ROS generated by the surrounding Gr1+ relatively mature myeloid cells via a paracrine mechanism (Figure 6A). To distinguish these two possibilities, we conducted a BM transplantation experiment in which TG-elicited expansion and differentiation of transplanted WT or CGD progenitors was investigated in CGD or WT recipient mice (Figure 6B). In order to examine the effect of BM myeloid cells on the proliferation of transplanted progenitor cells, non-irradiated mice were used as recipients. Disruption of NADPH did not affect the efficiency of donor cell engraftment. In both WT and CGD recipient mice, CD45.1 LK cells successfully engrafted with stable chimerism of about 0.4% over 6 weeks (Figure 6B). The TG-induced augmented proliferation of transplanted WT progenitors was abolished in the CGD recipient mice. In contrast, accelerated proliferation of transplanted CGD progenitors was detected in TG-challenged WT recipient mice (Figure 6C–D). These results suggest that the TG-elicited reactive granulopoiesis was mainly dependent on ROS production in the recipient mice,

demonstrating that BM myeloid cell derived ROS externally regulate reactive granulopoiesis via a paracrine mechanism.

Phagocytic NADPH oxidase may also be expressed in BM non-hematopoietic niche cells although the level is low. Thus some of the effects observed in the CGD mice may be due to NADPH oxidase disruption in niche cells. To rule out this possibility, we examined the sterile inflammation-induced expansion of the transplanted WT myeloid progenitors in lethally irradiated CGD recipients in which all the hematopoietic cells were derived from WT donor hematopoietic stem/progenitor cells (HSPCs) (Figure 7A). In this setup, the TG-elicited reactive granulopoiesis was still observed in CGD recipient mice, indicating that NADPH oxidase in BM non-hematopoietic cells was not involved in ROS-mediated reactive granulopoiesis (Figure 7B–C).

ROS are critical for reactive granulopoiesis induced by acid-elicited acute lung injury

BM myeloid cell-derived ROS play an important role in eliciting reactive granulopoiesis in a TG-induced sterile peritonitis model. Although this system is a widely used and accepted acute sterile inflammation model, it has only limited clinical relevance. Thus, for clinical correlation and to test the generalizability of our findings, we next explored the role of ROS in regulating reactive granulopoiesis in the acid-elicited acute lung injury model, another sterile inflammation model of greater clinical value.

Acid aspiration causes acute lung injury (ALI). Acid aspiration in mice, which mimics acid-elicited human ALI, was induced experimentally by intratracheal instillation of hydrochloric acid (HCl). Consistent with previous reports (35, 36), acid instillation resulted in the recruitment of significant numbers of neutrophils to the damaged lungs and caused acute sterile inflammation (Figure 8A). Similar to TG-elicited inflammation, acid-induced inflammation was associated with augmented ROS production in the BM extracellular space. Acid-induced BM ROS production was significantly suppressed in CGD mice, suggesting that these ROS were generated by phagocytic NADPH oxidase (Figure 8B). The severity of acid-induced lung inflammation measured by neutrophil recruitment was comparable between WT and CGD mice. Acid-induced ALI specifically expanded GMPs, an effect that was completely abolished in the CGD mice and confirming that reactive granulopoiesis induced by acid-elicited ALI was a phagocytic NADPH oxidase-dependent process (Figure 8C). In addition, a lower percentage of Edu+-proliferating cells was present in the GMP population of acid-challenged CGD mice compared to WT mice (Figure 8D). Finally, CFU-GM assay show that the number of myeloid progenitors in the BM did not increase in CGD mice, again suggesting that inhibition of NOX2-dependent ROS suppresses reactive granulopoiesis in acid-elicited ALI (Figure 8E). Taken together, our results demonstrate that ROS is the common pathway on which several clinically relevant non-infectious and infectious stimuli of emergency/reactive granulopoiesis converge despite their distinct primary stimuli and recognition pathways.

Discussion

At the early stage of inflammation, neutrophil mobilization from the BM leads to an immediate peripheral blood neutrophilia, which is followed by augmented BM

granulopoiesis to compensate for their peripheral loss. Here we show that although non-infectious stimuli-elicited reactive granulopoiesis and microbial infection-driven emergency granulopoiesis are triggered by different stimuli and there might also be fundamental molecular differences, NADPH oxidase-dependent ROS production is critical for both processes (Figure S3A). This also provides a novel therapeutic strategy for rebalancing neutrophil homeostasis in both physiologic and pathologic conditions, such as immune recovery after chemotherapy or after bone marrow transplantation.

The role of ROS in hematopoiesis is well documented (37–51). Most of these studies focus on ROS within stem or progenitor cells. In contrast, we show that microenvironmental rather than endogenous ROS contribute to stem and progenitor cells maintenance and proliferation during both pathogen-induced emergency granulopoiesis and sterile inflammation-induced reactive granulopoiesis (Figure S3A). The BM is the major myeloid reservoir. A large amount of ROS are generated by the Gr1+ myeloid cells in the BM during infection or inflammation. Currently, the factors that induce NOX2 activation and ROS generation during infection and inflammation are still ill-defined. Proinflammatory factors such as KC, MIP2, IL1, G-CSF, and TNFα can all activate NADPH oxidase and elevate ROS production. ROS are essential intracellular signaling molecules. They often regulate the structure and function of target proteins via post-translational thiol modifications including glutathionylation, nitrosylation, and sulfenic acid and disulfide bond formation (52–54). There are numerous ROS-target proteins such as protein kinases and phosphatases, actin, Ras GTPases, caspases, and transcription factors. Here we provide evidence that PTEN is a direct ROS target that plays a critical role in TG-induced reactive granulopoiesis. We demonstrate that oxidation-induced PTEN deactivation is not only essential but also sufficient to generate ROS-elicited phenotypes. However, we cannot rule out the possibility that other ROS-mediated pathways may also be involved in inflammation-induced emergency granulopoiesis.

G-CSF is a granulopoietic factor that is used clinically to produce granulocytes. G-CSF levels increase in infective and inflammatory conditions, and it is implicated in “steady-state” (55–57), pathogen-induced emergency granulopoiesis-triggered (11, 12), and sterile inflammation-elicited reactive granulopoiesis (9, 15). Intriguingly, TG-induced G-CSF expression (Figure S3B) and serum G-CSF levels (Figure S3C) were not suppressed in CGD mice, suggesting that G-CSF was not the major downstream ROS effector. Moreover, G-CSF signaling blockade with an anti-G-CSF antibody only caused a small reduction in bone marrow H_2O_2 in TG-challenged mice. TG treatment still induced significant ROS production even when G-CSF signaling was inhibited (Figure S3D). In addition, anti-G-CSF antibody treatment did not completely inhibit TG-elicited reactive granulopoiesis (Figure S3E). Finally, G-CSF-induced increases in ROS levels in the BM were much smaller than those induced by TG (Figure S4A) but still augmented granulopoiesis in CGD mice (22). Collectively, these results suggest that ROS and G-CSF regulate expansion and differentiation of myeloid progenitors in parallel, further highlighting the significance of a G-CSF-independent ROS signal in granulopoiesis.

HSCs are well known immediate targets of inflammatory signals (9). Infection and inflammation can either directly or indirectly modulate HSCs (25). Consistent with this, we

observed expansion of the LSK cell population in our TG-induced peritonitis model. However, unlike chronic inflammation-induced alterations in hematopoiesis, which are reported to be regulated by interferons (25, 58–60), acute inflammation-induced LSK cell expansion is likely to be independent of interferon signaling since acute inflammation did not alter serum interferon (α, β, or γ) levels (Figure S4B). It appears that acute inflammation-induced LSK cell expansion is also controlled by BM ROS, the physiologic significance of which is uncertain. It would be intriguing to see whether NADPH oxidase-dependent ROS production by BM myeloid cells plays a role in regulating HSC self-renewal and pluripotency. In addition, acute inflammation-elicited augmentation of cell proliferation is cell-type specific; the proliferation rate of CMPs and MEPs remained unaltered. The source of this specificity requires further clarification.

Supplementary Material

Refer to Web version on PubMed Central for supplementary material.

Acknowledgments

T. Cheng is supported by the grants from the Ministry of Science and Technology of China (2011CB964801) and from the Nature Science Foundation of China (81090411). Y. Xu is supported by the grants from National Basic Research Program of China (2012CB966403) and Chinese National Natural Sciences Foundation (No. 31271484), and Tianjin Natural Science Foundation (12JCZDJC24600). H. Luo is supported by NIH grants R01AI103142, R01HL092020, P01 HL095489 and a grant from the FAMRI.

The authors thank John Lucky and John Manis for helpful discussions, Dr. Christopher J. Chang for providing PF6-AM dye.

References

1. Paul F, Arkin Y, Giladi A, Jaitin DA, Kenigsberg E, Keren-Shaul H, Winter D, Lara-Astiaso D, Gury M, Weiner A, David E, Cohen N, Lauridsen FK, Haas S, Schlitzer A, Mildner A, Ginhoux F, Jung S, Trumpp A, Porse BT, Tanay A, Amit I. Transcriptional Heterogeneity and Lineage Commitment in Myeloid Progenitors. Cell. 2015; 163:1663–1677. [PubMed: 26627738]
2. Notta F, Zandi S, Takayama N, Dobson S, Gan OI, Wilson G, Kaufmann KB, McLeod J, Laurenti E, Dunant CF, McPherson JD, Stein LD, Dror Y, Dick JE. Distinct routes of lineage development reshape the human blood hierarchy across ontogeny. Science. 2016; 351:aab2116. [PubMed: 26541609]
3. Yamamoto R, Morita Y, Ooehara J, Hamanaka S, Onodera M, Rudolph KL, Ema H, Nakauchi H. Clonal analysis unveils self-renewing lineage-restricted progenitors generated directly from hematopoietic stem cells. Cell. 2013; 154:1112–1126. [PubMed: 23993099]
4. Kondo M, Wagers AJ, Manz MG, Prohaska SS, Scherer DC, Beilhack GF, Shizuru JA, Weissman IL. Biology of hematopoietic stem cells and progenitors: implications for clinical application. Annu Rev Immunol. 2003; 21:759–806. [PubMed: 12615892]
5. Ueda Y, Kondo M, Kelsoe G. Inflammation and the reciprocal production of granulocytes and lymphocytes in bone marrow. J Exp Med. 2005; 201:1771–1780. [PubMed: 15939792]
6. Ueda Y, Yang K, Foster SJ, Kondo M, Kelsoe G. Inflammation controls B lymphopoiesis by regulating chemokine CXCL12 expression. J Exp Med. 2004; 199:47–58. [PubMed: 14707114]
7. Zhang DE, Zhang P, Wang ND, Hetherington CJ, Darlington GJ, Tenen DG. Absence of granulocyte colony-stimulating factor signaling and neutrophil development in CCAAT enhancer binding protein alpha-deficient mice. Proc Natl Acad Sci U S A. 1997; 94:569–574. [PubMed: 9012825]
8. Hirai H, Zhang P, Dayaram T, Hetherington CJ, Mizuno S, Imanishi J, Akashi K, Tenen DG. C/EBPbeta is required for 'emergency' granulopoiesis. Nat Immunol. 2006; 7:732–739. [PubMed: 16751774]

9. Ueda Y, Cain DW, Kuraoka M, Kondo M, Kelsoe G. IL-1R type I-dependent hemopoietic stem cell proliferation is necessary for inflammatory granulopoiesis and reactive neutrophilia. J Immunol. 2009; 182:6477–6484. [PubMed: 19414802]
10. Manz MG, Boettcher S. Emergency granulopoiesis. Nat Rev Immunol. 2014; 14:302–314. [PubMed: 24751955]
11. Nagai Y, Garrett KP, Ohta S, Bahrun U, Kouro T, Akira S, Takatsu K, Kincade PW. Toll-like receptors on hematopoietic progenitor cells stimulate innate immune system replenishment. Immunity. 2006; 24:801–812. [PubMed: 16782035]
12. Boettcher S, Gerosa RC, Radpour R, Bauer J, Ampenberger F, Heikenwalder M, Kopf M, Manz MG. Endothelial cells translate pathogen signals into G-CSF-driven emergency granulopoiesis. Blood. 2014; 124:1393–1403. [PubMed: 24990886]
13. Boettcher S, Ziegler P, Schmid MA, Takizawa H, van Rooijen N, Kopf M, Heikenwalder M, Manz MG. Cutting edge: LPS-induced emergency myelopoiesis depends on TLR4-expressing nonhematopoietic cells. J Immunol. 2012; 188:5824–5828. [PubMed: 22586037]
14. Scumpia PO, Kelly-Scumpia KM, Delano MJ, Weinstein JS, Cuenca AG, Al-Quran S, Bovio I, Akira S, Kumagai Y, Moldawer LL. Cutting edge: bacterial infection induces hematopoietic stem and progenitor cell expansion in the absence of TLR signaling. J Immunol. 2010; 184:2247–2251. [PubMed: 20130216]
15. Cain DW, Snowden PB, Sempowski GD, Kelsoe G. Inflammation triggers emergency granulopoiesis through a density-dependent feedback mechanism. PLoS One. 2011; 6:e19957. [PubMed: 21655273]
16. Walker F, Zhang HH, Matthews V, Weinstock J, Nice EC, Ernst M, Rose-John S, Burgess AW. IL6/sIL6R complex contributes to emergency granulopoietic responses in G-CSF- and GM-CSF-deficient mice. Blood. 2008; 111:3978–3985. [PubMed: 18156493]
17. Caracciolo D, Clark SC, Rovera G. Human interleukin-6 supports granulocytic differentiation of hematopoietic progenitor cells and acts synergistically with GM-CSF. Blood. 1989; 73:666–670. [PubMed: 2644983]
18. Donahue RE, Seehra J, Metzger M, Lefebvre D, Rock B, Carbone S, Nathan DG, Garnick M, Sehgal PK, Laston D, et al. Human IL-3 and GM-CSF act synergistically in stimulating hematopoiesis in primates. Science. 1988; 241:1820–1823. [PubMed: 3051378]
19. Koike K, Stanley ER, Ihle JN, Ogawa M. Macrophage colony formation supported by purified CSF-1 and/or interleukin 3 in serum-free culture: evidence for hierarchical difference in macrophage colony-forming cells. Blood. 1986; 67:859–864. [PubMed: 3082388]
20. Hibbs ML, Quilici C, Kountouri N, Seymour JF, Armes JE, Burgess AW, Dunn AR. Mice lacking three myeloid colony-stimulating factors (G-CSF, GM-CSF, and M-CSF) still produce macrophages and granulocytes and mount an inflammatory response in a sterile model of peritonitis. J Immunol. 2007; 178:6435–6443. [PubMed: 17475873]
21. Nishinakamura R, Miyajima A, Mee PJ, Tybulewicz VL, Murray R. Hematopoiesis in mice lacking the entire granulocyte-macrophage colony-stimulating factor/interleukin-3/interleukin-5 functions. Blood. 1996; 88:2458–2464. [PubMed: 8839836]
22. Kwak HJ, Liu P, Bajrami B, Xu Y, Park SY, Nombela-Arrieta C, Mondal S, Sun Y, Zhu H, Chai L, Silberstein LE, Cheng T, Luo HR. Myeloid cell-derived reactive oxygen species externally regulate the proliferation of myeloid progenitors in emergency granulopoiesis. Immunity. 2015; 42:159–171. [PubMed: 25579427]
23. Jia Y, Subramanian KK, Erneux C, Pouillon V, Hattori H, Jo H, You J, Zhu D, Schurmans S, Luo HR. Inositol 1,3,4,5-tetrakisphosphate negatively regulates phosphatidylinositol-3,4,5-trisphosphate signaling in neutrophils. Immunity. 2007; 27:453–467. [PubMed: 17825589]
24. Subramanian KK, Jia Y, Zhu D, Simms BT, Jo H, Hattori H, You J, Mizgerd JP, Luo HR. Tumor suppressor PTEN is a physiologic suppressor of chemoattractant-mediated neutrophil functions. Blood. 2007; 109:4028–4037. [PubMed: 17202315]
25. King KY, Goodell MA. Inflammatory modulation of HSCs: viewing the HSC as a foundation for the immune response. Nat Rev Immunol. 2011; 11:685–692. [PubMed: 21904387]

26. Zhang P, Nelson S, Bagby GJ, Siggins R 2nd, Shellito JE, Welsh DA. The lineage-c-Kit+Sca-1+ cell response to Escherichia coli bacteremia in Balb/c mice. Stem Cells. 2008; 26:1778–1786. [PubMed: 18483422]
27. Subramanian, KK., Luo, HR. Non-classical roles of NADPH-oxidase dependent Reactive Oxygen Species in Phagocytes. In: Kohlund, RHaS, editor. Granulocytes: Classification, Toxic Materials Produced and Pathology. Nova Science Publishers, Inc; 2009.
28. Dinauer MC. Chronic granulomatous disease and other disorders of phagocyte function. Hematology Am Soc Hematol Educ Program. 2005:89–95. [PubMed: 16304364]
29. Pollock JD, Williams DA, Gifford MA, Li LL, Du X, Fisherman J, Orkin SH, Doerschuk CM, Dinauer MC. Mouse model of X-linked chronic granulomatous disease, an inherited defect in phagocyte superoxide production. Nat Genet. 1995; 9:202–209. [PubMed: 7719350]
30. Hattori H, Subramanian KK, Sakai J, Jia Y, Li Y, Porter TF, Loison F, Sarraj B, Kasorn A, Jo H, Blanchard C, Zirkle D, McDonald D, Pai SY, Serhan CN, Luo HR. Small-molecule screen identifies reactive oxygen species as key regulators of neutrophil chemotaxis. Proc Natl Acad Sci U S A. 2010; 107:3546–3551. [PubMed: 20142487]
31. Yilmaz OH, Valdez R, Theisen BK, Guo W, Ferguson DO, Wu H, Morrison SJ. Pten dependence distinguishes haematopoietic stem cells from leukaemia-initiating cells. Nature. 2006; 441:475–482. [PubMed: 16598206]
32. Zhang J, Grindley JC, Yin T, Jayasinghe S, He XC, Ross JT, Haug JS, Rupp D, Porter-Westpfahl KS, Wiedemann LM, Wu H, Li L. PTEN maintains haematopoietic stem cells and acts in lineage choice and leukaemia prevention. Nature. 2006; 441:518–522. [PubMed: 16633340]
33. Silva A, Yunes JA, Cardoso BA, Martins LR, Jotta PY, Abecasis M, Nowill AE, Leslie NR, Cardoso AA, Barata JT. PTEN posttranslational inactivation and hyperactivation of the PI3K/Akt pathway sustain primary T cell leukemia viability. J Clin Invest. 2008; 118:3762–3774. [PubMed: 18830414]
34. Rommel C, Camps M, Ji H. PI3K delta and PI3K gamma: partners in crime in inflammation in rheumatoid arthritis and beyond? Nat Rev Immunol. 2007; 7:191–201. [PubMed: 17290298]
35. Zarbock A, Singbartl K, Ley K. Complete reversal of acid-induced acute lung injury by blocking of platelet-neutrophil aggregation. J Clin Invest. 2006; 116:3211–3219. [PubMed: 17143330]
36. Abdulnour RE, Dalli J, Colby JK, Krishnamoorthy N, Timmons JY, Tan SH, Colas RA, Petasis NA, Serhan CN, Levy BD. Maresin 1 biosynthesis during platelet-neutrophil interactions is organ-protective. Proc Natl Acad Sci U S A. 2014; 111:16526–16531. [PubMed: 25369934]
37. Rhee SG. Cell signaling. H2O2, a necessary evil for cell signaling. Science. 2006; 312:1882–1883. [PubMed: 16809515]
38. Finkel T. Reactive oxygen species and signal transduction. IUBMB Life. 2001; 52:3–6. [PubMed: 11795590]
39. Dickinson BC, Chang CJ. Chemistry and biology of reactive oxygen species in signaling or stress responses. Nat Chem Biol. 2011; 7:504–511. [PubMed: 21769097]
40. Veal EA, Day AM, Morgan BA. Hydrogen peroxide sensing and signaling. Mol Cell. 2007; 26:1–14. [PubMed: 17434122]
41. Nathan C, Cunningham-Bussel A. Beyond oxidative stress: an immunologist's guide to reactive oxygen species. Nat Rev Immunol. 2013; 13:349–361. [PubMed: 23618831]
42. Jang YY, Sharkis SJ. A low level of reactive oxygen species selects for primitive hematopoietic stem cells that may reside in the low-oxygenic niche. Blood. 2007; 110:3056–3063. [PubMed: 17595331]
43. Ito K, Hirao A, Arai F, Takubo K, Matsuoka S, Miyamoto K, Ohmura M, Naka K, Hosokawa K, Ikeda Y, Suda T. Reactive oxygen species act through p38 MAPK to limit the lifespan of hematopoietic stem cells. Nat Med. 2006; 12:446–451. [PubMed: 16565722]
44. Ito K, Hirao A, Arai F, Matsuoka S, Takubo K, Hamaguchi I, Nomiyama K, Hosokawa K, Sakurada K, Nakagata N, Ikeda Y, Mak TW, Suda T. Regulation of oxidative stress by ATM is required for self-renewal of haematopoietic stem cells. Nature. 2004; 431:997–1002. [PubMed: 15496926]
45. Haneline LS. Redox regulation of stem and progenitor cells. Antioxid Redox Signal. 2008; 10:1849–1852. [PubMed: 18665798]

46. Lewandowski D, Barroca V, Duconge F, Bayer J, Van Nhieu JT, Pestourie C, Fouchet P, Tavitian B, Romeo PH. In vivo cellular imaging pinpoints the role of reactive oxygen species in the early steps of adult hematopoietic reconstitution. Blood. 2010; 115:443–452. [PubMed: 19797522]
47. Gupta R, Karpatkin S, Basch RS. Hematopoiesis and stem cell renewal in long-term bone marrow cultures containing catalase. Blood. 2006; 107:1837–1846. [PubMed: 16278309]
48. Owusu-Ansah E, Banerjee U. Reactive oxygen species prime Drosophila haematopoietic progenitors for differentiation. Nature. 2009; 461:537–541. [PubMed: 19727075]
49. Hole PS, Pearn L, Tonks AJ, James PE, Burnett AK, Darley RL, Tonks A. Ras-induced reactive oxygen species promote growth factor-independent proliferation in human CD34+ hematopoietic progenitor cells. Blood. 2010; 115:1238–1246. [PubMed: 20007804]
50. Zhu QS, Xia L, Mills GB, Lowell CA, Touw IP, Corey SJ. G-CSF induced reactive oxygen species involves Lyn-PI3-kinase-Akt and contributes to myeloid cell growth. Blood. 2006; 107:1847–1856. [PubMed: 16282349]
51. Juntilla MM, Patil VD, Calamito M, Joshi RP, Birnbaum MJ, Koretzky GA. AKT1 and AKT2 maintain hematopoietic stem cell function by regulating reactive oxygen species. Blood. 2010; 115:4030–4038. [PubMed: 20354168]
52. Ghezzi P. Oxidoreduction of protein thiols in redox regulation. Biochem Soc Trans. 2005; 33:1378–1381. [PubMed: 16246123]
53. Shelton MD, Chock PB, Mieyal JJ. Glutaredoxin: role in reversible protein s-glutathionylation and regulation of redox signal transduction and protein translocation. Antioxid Redox Signal. 2005; 7:348–366. [PubMed: 15706083]
54. Janssen-Heininger YM, Mossman BT, Heintz NH, Forman HJ, Kalyanaraman B, Finkel T, Stamler JS, Rhee SG, van der Vliet A. Redox-based regulation of signal transduction: principles, pitfalls, and promises. Free Radic Biol Med. 2008; 45:1–17. [PubMed: 18423411]
55. Smith E, Zarbock A, Stark MA, Burcin TL, Bruce AC, Foley P, Ley K. IL-23 is required for neutrophil homeostasis in normal and neutrophilic mice. J Immunol. 2007; 179:8274–8279. [PubMed: 18056371]
56. Stark MA, Huo Y, Burcin TL, Morris MA, Olson TS, Ley K. Phagocytosis of apoptotic neutrophils regulates granulopoiesis via IL-23 and IL-17. Immunity. 2005; 22:285–294. [PubMed: 15780986]
57. Basu S, Hodgson G, Zhang HH, Katz M, Quilici C, Dunn AR. “Emergency” granulopoiesis in G-CSF-deficient mice in response to Candida albicans infection. Blood. 2000; 95:3725–3733. [PubMed: 10845903]
58. MacNamara KC, Oduro K, Martin O, Jones DD, McLaughlin M, Choi K, Borjesson DL, Winslow GM. Infection-induced myelopoiesis during intracellular bacterial infection is critically dependent upon IFN-gamma signaling. J Immunol. 2011; 186:1032–1043. [PubMed: 21149601]
59. Sato T, Onai N, Yoshihara H, Arai F, Suda T, Ohteki T. Interferon regulatory factor-2 protects quiescent hematopoietic stem cells from type I interferon-dependent exhaustion. Nat Med. 2009; 15:696–700. [PubMed: 19483695]
60. Baldridge MT, King KY, Boles NC, Weksberg DC, Goodell MA. Quiescent haematopoietic stem cells are activated by IFN-gamma in response to chronic infection. Nature. 2010; 465:793–797. [PubMed: 20535209]
61. Loison F, Zhu H, Karatepe K, Kasorn A, Liu P, Ye K, Zhou J, Cao S, Gong H, Jenne DE, Remold-O’Donnell E, Xu Y, Luo HR. Proteinase 3-dependent caspase-3 cleavage modulates neutrophil death and inflammation. J Clin Invest. 2014; 124:4445–4458. [PubMed: 25180606]
62. Li Y, Prasad A, Jia Y, Roy SG, Loison F, Mondal S, Kocjan P, Silberstein LE, Ding S, Luo HR. Pretreatment with phosphatase and tensin homolog deleted on chromosome 10 (PTEN) inhibitor SF1670 augments the efficacy of granulocyte transfusion in a clinically relevant mouse model. Blood. 2011; 117:6702–6713. [PubMed: 21521784]
63. Liang OD, Lu J, Nombela-Arrieta C, Zhong J, Zhao L, Pivarnik G, Mondal S, Chai L, Silberstein LE, Luo HR. Deficiency of lipid phosphatase SHIP enables long-term reconstitution of hematopoietic inductive bone marrow microenvironment. Dev Cell. 2013; 25:333–349. [PubMed: 23725762]
64. Mazo IB, Gutierrez-Ramos JC, Frenette PS, Hynes RO, Wagner DD, von Andrian UH. Hematopoietic progenitor cell rolling in bone marrow microvessels: parallel contributions by

endothelial selectins and vascular cell adhesion molecule 1. J Exp Med. 1998; 188:465–474. [PubMed: 9687524]

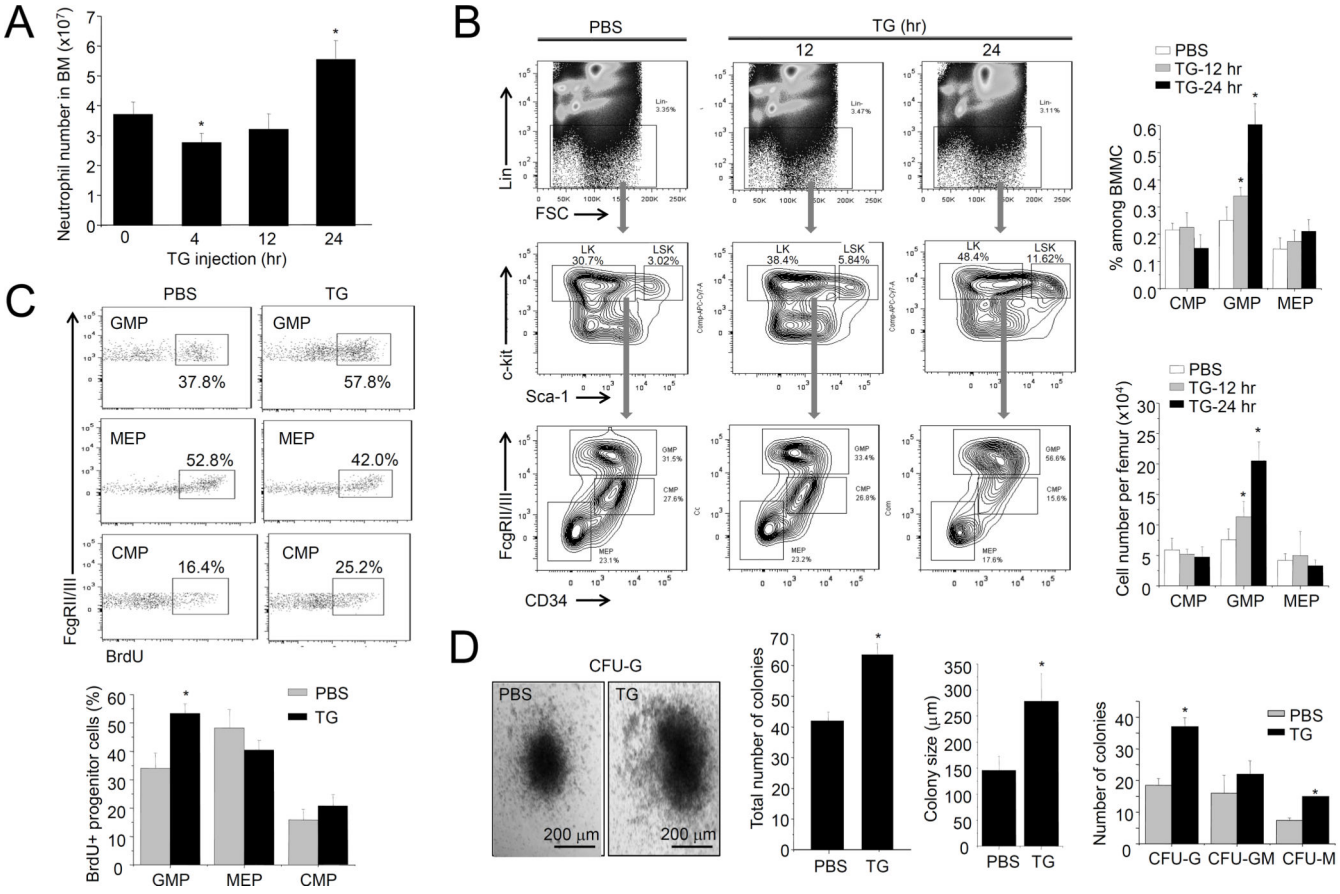

Figure 1. TG-induced sterile inflammation leads to increased progenitor cell proliferation in the BM

(A) The number of neutrophils in the BM was measured using the Wright-Giemsa staining method. Data shown are means ± SD of n=5 mice. * p<0.01 versus control. **(B)** Flow cytometry-based lineage analysis of the BM cells. The percentage of each cell population among BM-derived mononuclear cells (BMMCs), and the absolute cell number per femur, are shown. Data shown are means ± SD of n=5 mice. * p<0.01 versus control (PBS treated mice). **(C)** Measurement of cycling cells in each progenitor population by incorporation of BrdU. Data shown are means ± SD of n=5 mice. * p<0.01 versus control. (**D**) The number of myeloid progenitors analyzed using an *in vitro* CFU-GM colony-forming assay. Data are means ± SD of n=5 mice. Representative pictures of cell clusters/colonies are shown.

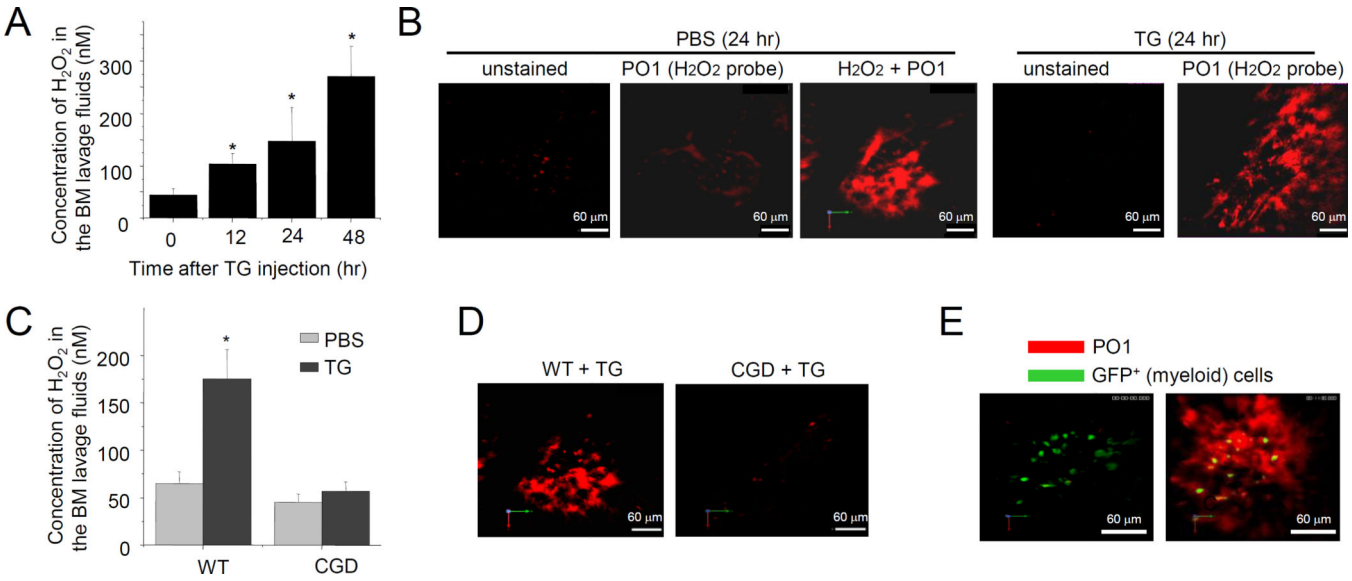

Figure 2. Hydrogen peroxide (H_2O_2) levels increase in the BM during TG-elicited acute inflammation

(A) BM extracellular ROS measured using the Amplex® Red assay. Data shown are means ± SD of n=5 mice. * p<0.01 versus time 0. **(B)** Measurement of BM hydrogen peroxide using two-photon intravital microscopy. **(C)** Acute inflammation-elicited elevation of ROS production in the BM was abolished in CGD mice (24 hr after TG injection). Data shown are means ± SD of n=5 mice. * p<0.01. **(D)** The extracellular ROS was measured with PO1 dye using two-photon intravital microscopy, 24 hr after the TG treatment. Shown are representative pictures of three independent experiments. **(E)** H_2O_2 was adjacent to myeloid cells in the bone marrow. H_2O_2 was measured with PO1 dye using two-photon intravital microscopy in LyzM-EGFP mice.

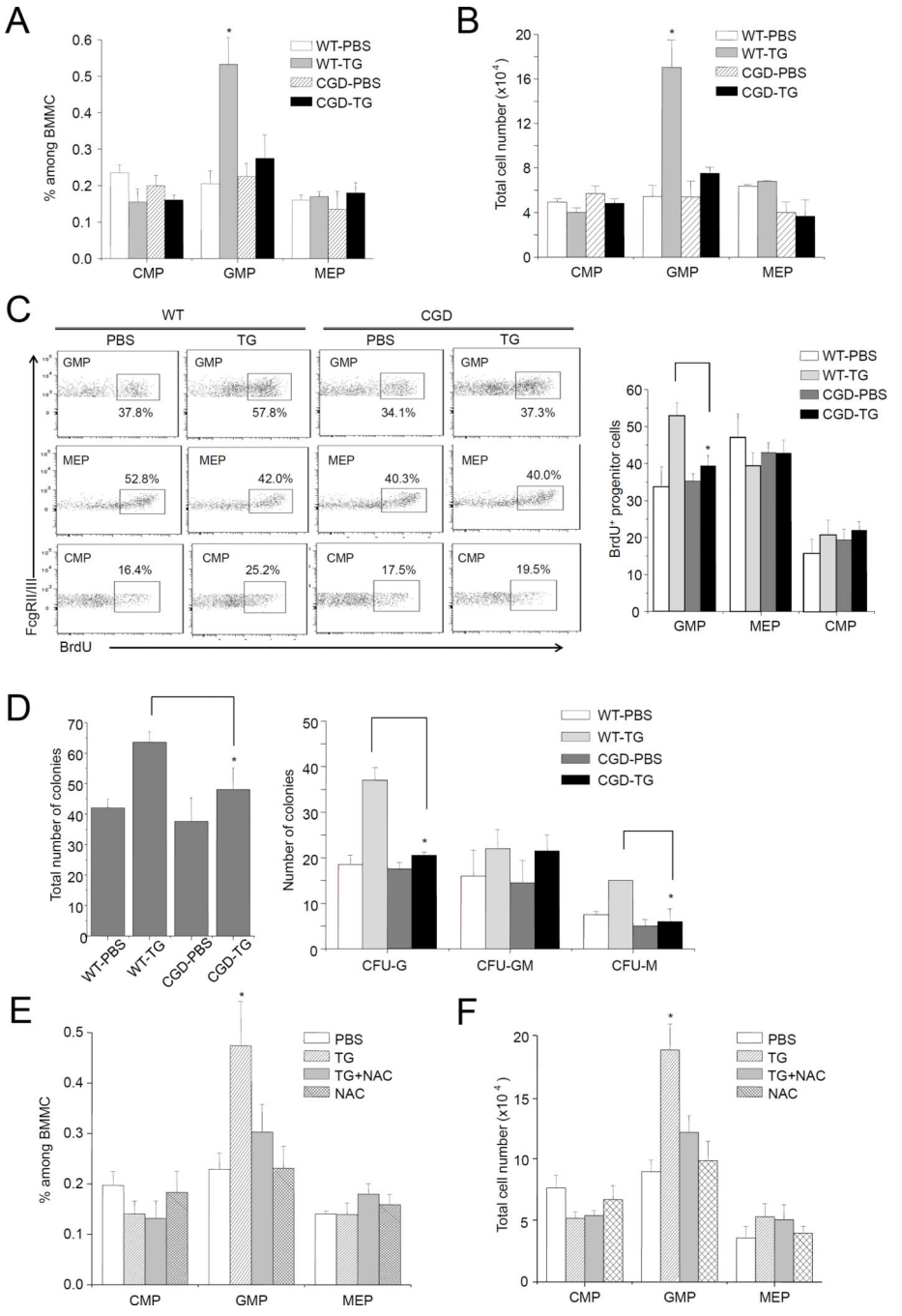

Figure 3. NADPH oxidase-mediated ROS production is essential for TG-induced reactive granulopoiesis

(A) Inflammation-induced elevation of myeloid progenitor subset depends on phagocyte NADPH oxidase. Flow cytometry-based lineage analysis was conducted in WT and CGD mice 24 hr after TG injection. The percentage of each cell population among BMMCs was measured as described in Figure 1. **(B)** The absolute cell number of indicated cells per femur. Data represent the mean ± SD of n=4 mice per group. * p<0.01 versus PBS control. **(C)** Proliferation of progenitor cells in WT and CGD mice during inflammation was

determined by BrdU incorporation. The WT data (also shown in Figure 1C) were included for comparison purpose. (**D**) The number of myeloid progenitors analyzed using an *in vitro* CFU-GM colony-forming assay. Data shown are mean ± SD of n=5 mice. * $p<0.01$ versus CGD. **(E)** Flow cytometry-based lineage analysis. Mice were treated with NAC (100 mg/kg, ip) 3 hr before TG injection. Twenty-four hr after TG injection, BM cells were isolated and analyzed. The percentage of each cell population among BMMCs was measured as described in Figure 1. **(F)** The absolute cell number of indicated cells per femur ($n=5$ for each group). * $p<0.01$ versus PBS control.

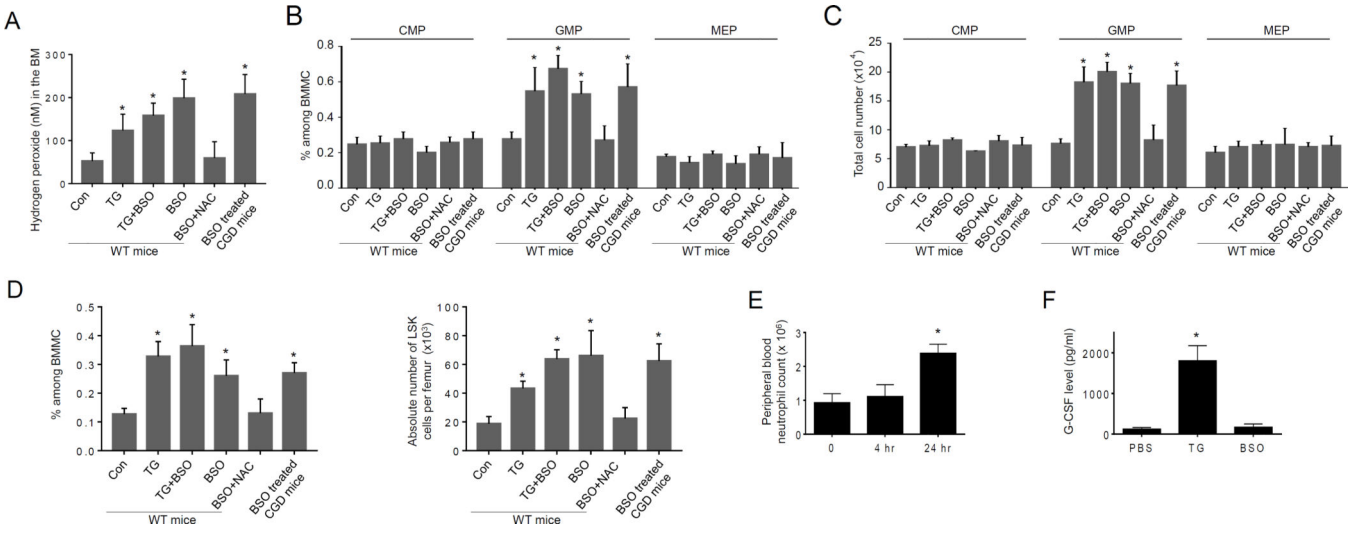

Figure 4. ROS accelerate proliferation of myeloid progenitor cells to levels comparable to TG-induced granulopoiesis

(A) Treatment with BSO elevates ROS level in the BM. WT or CGD mice were treated with BSO (10 mg/kg, ip) 3 hr before TG injection. When NAC was used, it (100 mg/kg, ip) was applied together with BSO. The level of H_2O_2 in the BM was quantified 20 hr after the TG injection as described in Figure 2A. Data shown are means ± SD of n=5 mice. *p<0.01 versus mice injected with PBS alone. **(B–C)** ROS promote granulopoiesis *in vivo*. Flow-cytometry based lineage analysis of the BM cells was conducted 24 hr after TG injection. The percentage of each cell population among BM-derived mononuclear cells **(B)** and the absolute cell number per femur **(C)** are shown. Data represent the means ± SD of n = 5 mice per group. * p<0.01 versus PBS control. **(D)** Treatment with BSO leads to expansion of BM LSK cells. BSO treatment and induction of peritonitis with TG were carried out as described in Figure 4A. The flow-cytometry based lineage analysis were conducted 24 hr after TG injection as described in Figure 1B. Data shown are mean ± SD of n=5 mice. *p<0.01 versus mice injected with PBS alone. **(E)** Peripheral blood neutrophil counts in BSO treated mice. The peripheral blood neutrophil counts were measured as described in Figure S1A. Data shown are mean ± SD of n=5 mice. *p<0.01 versus mice injected with PBS alone. **(F)** Treatment with BSO does not induce G-CSF production. BSO treatment and induction of peritonitis with TG were carried out as described in Figure 4A. The serum G-CSF level was measured 24 hr after the injection using an ELISA Kit following the protocol provided by the manufacturer (R&D Systems, Inc. Minneapolis, MN). Data shown are mean ± SD of n=5 mice. *p<0.01 versus mice injected with PBS.

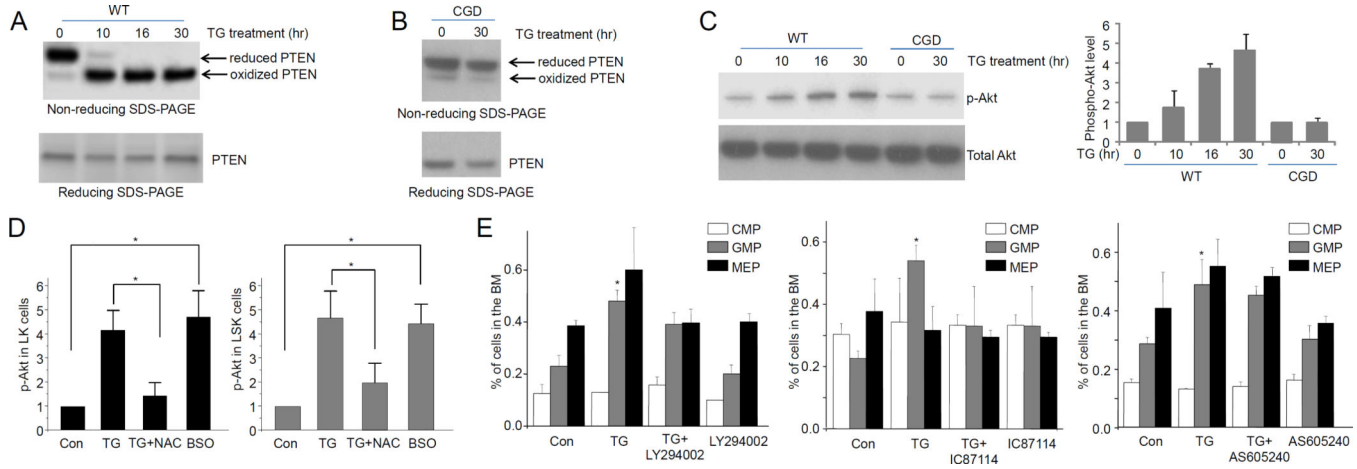

Figure 5. TG-induced reactive granulopoiesis is mediated by ROS-elicited deactivation of PTEN and subsequent Akt activation

(A) TG-elicited sterile inflammation induces PTEN oxidation in hematopoietic progenitor cells. The protein lysates from 0.5×10^6 LK cells (from 3 mice) were resolved using non-reducing SDS-PAGE. Reduced and oxidized forms of PTEN are indicated. Data shown are representative of multiple experiments with similar results. **(B)** TG-elicited PTEN oxidation is abolished in CGD hematopoietic progenitor cells. **(C)** TG-elicited acute inflammation leads to Akt activation in hematopoietic progenitor cells. Akt phosphorylation was expressed as ratio of phospho-Akt to total Akt. Data represent the means ± SD of n=5 mice per group. **(D)** ROS are both required and sufficient for inflammation-induced Akt phosphorylation. Mice were treated with NAC (100 mg/kg, ip) 3 hr before TG injection. Twenty-four hours after TG injection, Akt phosphorylation in hematopoietic progenitor cells (LK) was analyzed as described above. For BSO treatment, Akt phosphorylation in hematopoietic progenitor cells (LK) was analyzed 27 hr after the BSO (10 mg/kg, ip) injection. Data represent the means ± SD of n=5 mice per group. * p<0.01. **(E)** Inhibition of PtdIns(3,4,5)P3 signaling suppresses inflammation-induced granulopoiesis. Mice were either untreated or treated with PI3 kinase inhibitors LY294002 (i.p. 50 mg/kg body weight), IC87114 (i.p. 25 mg/kg body weight), or AS605240 (i.p. 50 mg/kg body weight) and then challenged with TG for 24 hr. Shown are the percentage of each cell population among BMMCs. Data represent the means ± SD of n=5 mice per group. * p<0.01 versus PBS control.

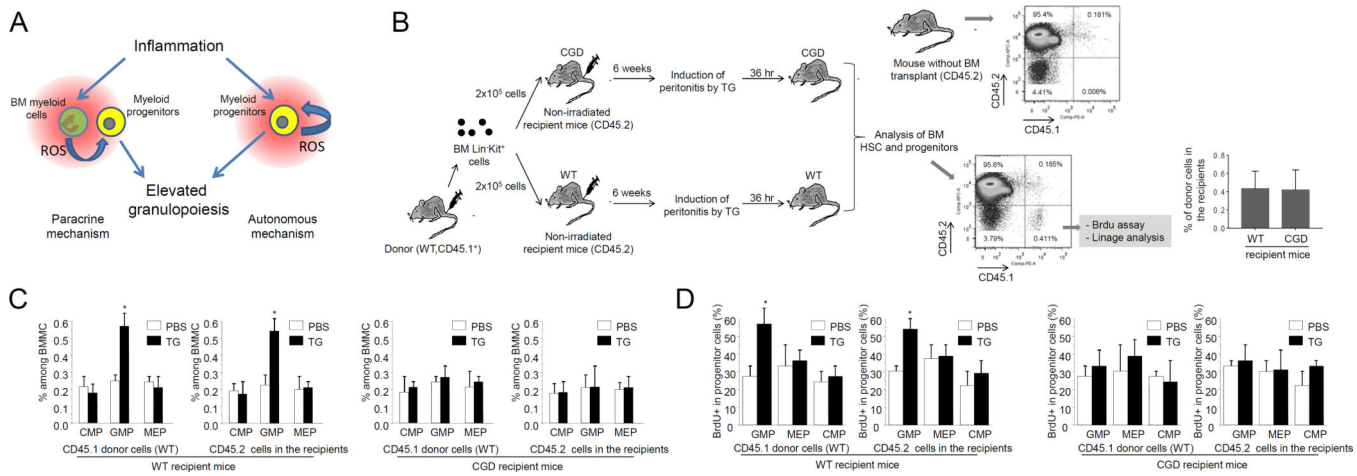

Figure 6. ROS regulate TG-induced reactive granulopoiesis via a paracrine mechanism

(A) ROS may regulate reactive granulopoiesis both autonomously and non-autonomously. **(B)** The schematic of the BM transplantation experiment. The percentages of donor derived (CD45.1+) cells among PB mononuclear cells in WT and CGD mice are shown. Data represent the means ± SD of $n = 5$ mice per group. **(C)** Flow cytometry-based lineage analysis of the CD45.1 (donor) and CD45.2 (recipient) BM cells. Data shown are mean ± SD of n=5 mice. * p<0.01 versus control (PBS treated mice). **(D)** Measurement of cycling cells in each progenitor population by incorporation of BrdU. Data shown are means ± SD of n=5 mice. * p<0.01versus control (PBS treated mice).

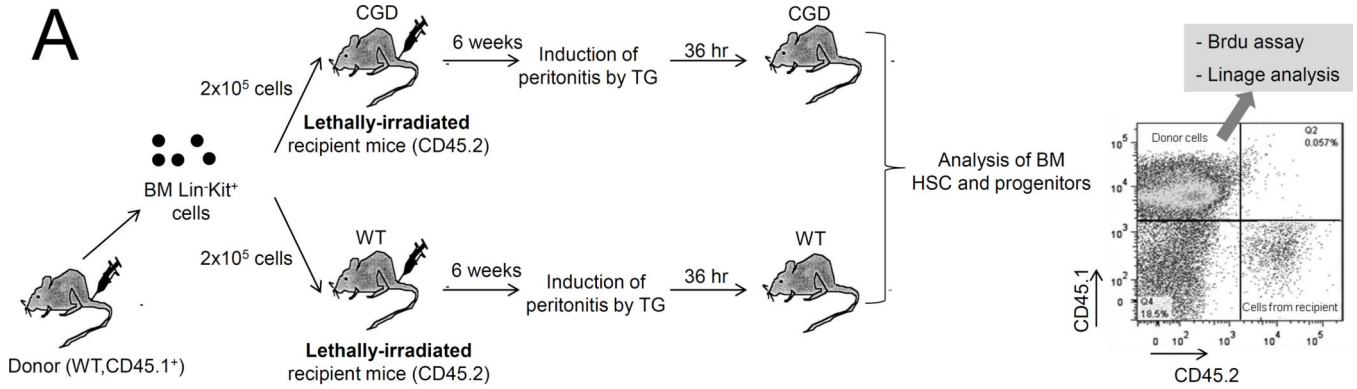

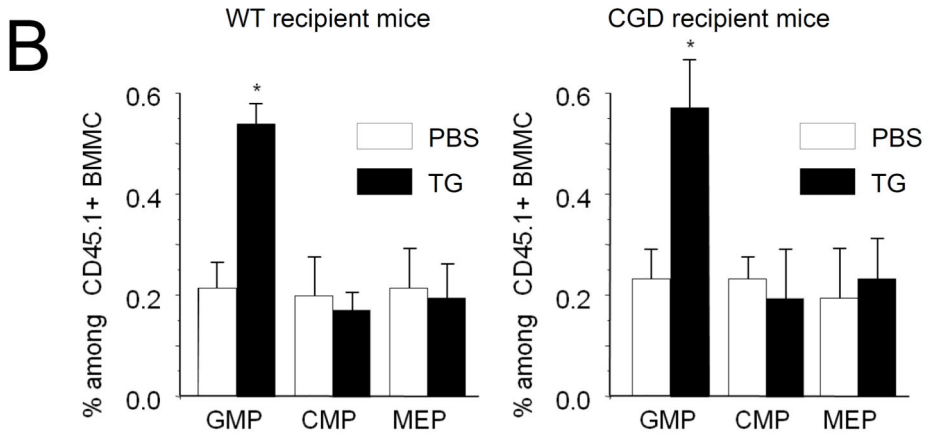

Figure 7. ROS produced by BM mesenchymal cells are not involved in reactive granulopoiesis

(A) The schematic of the BM transplantation experiment. Eight week-old WT and CGD mice were lethally irradiated with a dose of 10.2 Gy (two split doses of 5.1 Gy 4 hr apart) using a Cesium-137 Gamma animal irradiator. BM LinKit^{+} cells were obtained by flow cytometry sorting, and were injected into the lethally irradiated recipients intravenously. Bone marrow reconstitution was confirmed 6 weeks after the BM transplantation. **(B)** Flow cytometry-based lineage analysis of the CD45.1^{+} (donor) BM cells. The experiments were conducted and analyzed as described in Figure 6C. Data shown are means ± SD of three

experiments. * p<0.01versus control (PBS treated mice). **(C)** Measurement of cycling cells in each CD45.1^{+} progenitor population by incorporation of BrdU. The experiments were conducted as described in Figure 6D. Data shown are means ± SD of n=3 mice. * p<0.01versus control.

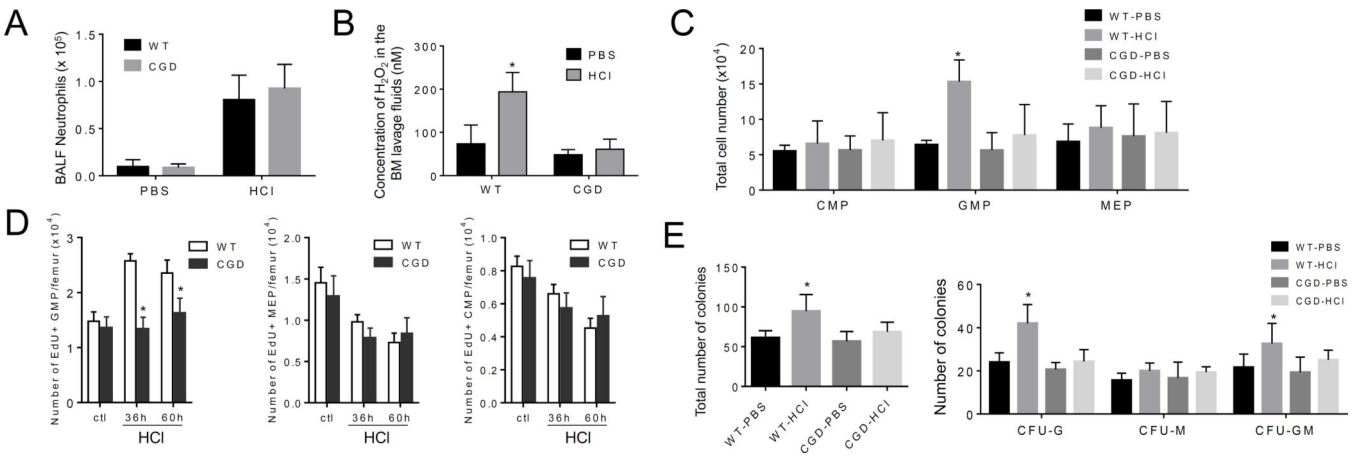

Figure 8. NADPH oxidase-mediated ROS production in the BM is critical for proliferation of myeloid progenitors during acid-elicited acute lung injury

(A) Neutrophil recruitment to the lungs during acid-elicited acute lung injury. The experiments were conducted 48 hr after the acid treatment. Data shown are means ± SD of n=5 mice. **(B)** BM extracellular ROS measured using the Amplex® Red assay. Data shown are means ± SD of n=5 mice. * p<0.01 versus PBS treated mice. **(C)** Acid-induced elevation of myeloid progenitor subset depends on phagocyte NADPH oxidase. Flow cytometry-based lineage analysis was conducted in WT and CGD mice 48 hr after acid instillation. Data shown are means ± SD of n=5 mice. * p<0.01 versus PBS treated mice. **(D)** Proliferation of progenitor cells in WT and CGD mice during acid-elicited acute lung injury was determined by EdU incorporation. Shown are the numbers of indicated progenitor cells in each femur. Data are means ± SD of n=5 mice. * p<0.01 versus PBS treated mice. (**E**) The number of myeloid progenitors analyzed using an *in vitro* CFU-GM colony-forming assay. Data shown are mean ± SD of n=5 mice. * p<0.01 versus PBS treated WT mice.